Proceedings of the
44th IEEE Conference on Decision and Control, and
the European Control Conference 2005
Seville, Spain, December 12-15, 2005



# Experimental output regulation for the TORA system

Alexey Pavlov, Bart Janssen, Nathan van de Wouw and Henk Nijmeijer

*Abstract*— **Research on the output regulation problem is mainly focused on theoretical developments and studies on simulation level. In this paper we present experimental results on the nonlinear output regulation problem for a benchmark mechanical system, the so-called TORA system. The effectiveness of the approach is shown and its practical limitations are illuminated.**

## I. INTRODUCTION

The output regulation problem is one of the most important problems in control theory. It includes the problems of tracking reference signals and rejecting disturbances generated by an external autonomous system (exosystem). For linear systems, this problem was thoroughly investigated in the 1970-s, see e.g. [1], [2]. For nonlinear systems, intensive research started with the papers [3] and [4], which provided solutions to the local output regulation problem for general nonlinear systems. These papers were followed by a number of results dealing with different aspects of the output regulation problem for nonlinear systems: approximate, robust and adaptive output regulation. For the latest list of references on the subject the reader is referred to the recent monographs [5], [6]. Despite the significant interest to this problem, most of the known results are theoretical and the proposed controllers solving the problem are validated only in simulations. To the best of our knowledge, at the moment there are only two publications [7] and [8] related to experimental output regulation for nonlinear systems. This motivates further studies in experimental nonlinear output regulation.

In this paper we present experimental results on output regulation for the so-called TORA system (Translational Oscillator with a Rotational Actuator). This system is a benchmark mechanical system used for testing many nonlinear control techniques, see e.g. [9], [10]. The local nonlinear output regulation problem for the TORA system has been considered in [11], [12]. First, in Section II we describe the TORA system and state a local disturbance rejection problem for this system. This problem is a particular case of the local nonlinear output regulation problem. In Section III a controller solving the disturbance rejection problem is presented. The experimental setup is described in Section IV. In Section V we present and discuss experimental results. Section VI contains conclusions. The results presented in this paper are part of the work [13].

This work was supported by Netherlands organization for scientific research NWO

A. Pavlov is with Department of Engineering Cybernetics, Norwegian University of Science and Technology, NO-7491, Trondheim, Norway. B. Janssen, N. van de Wouw and H. Nijmeijer are with Department of Mechanical Engineering, Eindhoven University of Technology, P.O. Box 513, 5600 MB, Eindhoven, The Netherlands. Alexey.Pavlov@itk.ntnu.no, B.R.A.Janssen@student.tue.nl, N.v.d.Wouw@tue.nl, H.Nijmeijer@tue.nl

## II. OUTPUT REGULATION OF THE TORA SYSTEM

Consider the so-called TORA-system (Transitional Oscillator with a Rotational Actuator), which is shown in Fig. 1. This system consists of a cart of mass $M$ which is attached to a wall with a spring of stiffness $k$. The cart is excited by a disturbance force $F_d$. In the center of the cart, there is a rotating arm of mass $m$. The center of mass of the arm CM is located at a distance of $l$ from the rotational axis and the arm has an inertia $J$ with respect to this axis. The arm is actuated by a control torque $T_u$. The cart and the arm move in the horizontal plane and, therefore, gravity effects are omitted. The horizontal displacement of the cart is denoted by $e$ and the angular displacement of the arm is denoted by $\theta$.

The control problem is to find a control law for the torque $T_u$ such that the horizontal displacement $e$ tends to zero in presence of a harmonic disturbance force $F_d$. The frequency of the disturbance force is fixed and known in advance, while the amplitude and phase may vary from experiment to experiment. This is a particular case of the output regulation problem. Firstly we find a controller solving this problem locally, i.e. for small initial conditions $e(0)$, $\dot{e}(0)$, $\theta(0)$, and $\dot{\theta}(0)$ and for disturbances with small amplitudes.

## III. CONTROLLER DESIGN FOR THE TORA SYSTEM

In this section we design a simple controller for the disturbance rejection problem considered in Section II. The equations of motion for the TORA system are given by [9]:

$$\begin{aligned} \bar{M}\ddot{e} + ml(\ddot{\theta}\cos\theta - \dot{\theta}^2\sin\theta) + ke &= F_d, \\ J\ddot{\theta} + ml\ddot{e}\cos\theta &= T_u, \end{aligned} \tag{1}$$

where $\bar{M} := M + m$. The disturbance force $F_d$ is generated by the linear exosystem

$$\dot{w}_1 = \omega w_2, \quad \dot{w}_2 = -\omega w_1, \quad F_d = w_1, \tag{2}$$

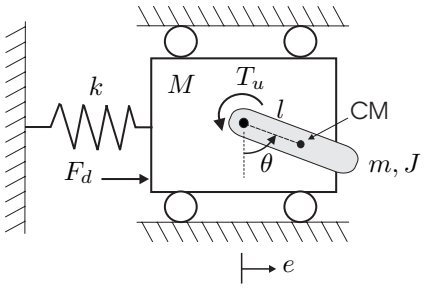


Fig. 1. The TORA system.

0-7803-9568-9/05/$20.00 ©2005 IEEE

where $\omega$ is the oscillation frequency. The initial conditions of the exosystem (2) determine the amplitude and phase of the excitation. The control problem is to asymptotically regulate $e(t)$ to zero for all sufficiently small initial conditions of the closed-loop system and for all sufficiently small initial conditions of the exosystem and at the same time to guarantee that for $F_d = 0$ the closed-loop system has an asymptotically stable linearization at the origin. This is a particular case of the local output regulation problem, see e.g. [14], [15]. We assume that $e$, $\dot{e}$, $\theta$, $\dot{\theta}$, $w_1$ and $w_2$ are measured and all parameters of the system are known.

Following [14], we seek a controller solving this problem in the form

$$T_u = c(w) + K(x - \pi(w)), \tag{3}$$

where $x := [e, \dot{e}, \theta, \dot{\theta}]^T$ is the state of the system (1) and $w := [w_1, w_2]^T$ is the state of the exosystem (2). The matrix $K$ is such that for $w = 0$ the closed-loop system (1), (3) has an asymptotically stable linearization at the origin. The mappings $\pi(w) := [\pi_1(w), \pi_2(w), \pi_3(w), \pi_4(w)]^T$ and $c(w)$, with $\pi(0) = 0$ and $c(0) = 0$, are $C^1$ mappings which are defined in a neighborhood of the origin $w = 0$ and satisfy the so-called regulator equations [15]. The solutions to the regulator equations have the following meaning: for any sufficiently small solution of the exosystem $w(t)$, for the disturbance force $F_d(t) = w_1(t)$ and controller action $T_u(t) = c(w(t))$, the function $x(t) = \pi(w(t))$ is a solution of system (1) and along this solution the displacement $e(t)$ equals zero. By substitution one can easily check that the mappings

$$\pi_1(w) = 0,\ \pi_2(w) = 0,\ \pi_3(w) = -\arcsin\left(\frac{w_1}{ml\omega^2}\right), \tag{4}$$

$$\pi_4(w) = -\frac{\omega w_2}{(m^2l^2\omega^4 - w_1^2)^{1/2}}, \tag{5}$$

$$c(w) = \frac{\omega^2 w_1 (m^2l^2\omega^4 - w_1^2 - w_2^2)J}{(m^2l^2\omega^4 - w_1^2)^{3/2}} \tag{6}$$

satisfy the regulator equations.

The requirement on the matrix $K$ is equivalent to the requirement that $A + BK$ is a Hurwitz matrix, where the matrices

$$A := \begin{bmatrix} 0 & 1 & 0 & 0 \\ -\frac{kJ}{\bar{M}J - m^2l^2} & 0 & 0 & 0 \\ 0 & 0 & 0 & 1 \\ \frac{kml}{\bar{M}J - m^2l^2} & 0 & 0 & 0 \end{bmatrix},\ B := \begin{bmatrix} 0 \\ -\frac{ml}{\bar{M}J - m^2l^2} \\ 0 \\ \frac{\bar{M}}{\bar{M}J - m^2l^2} \end{bmatrix}$$

follow from the linearization of system (1) at the origin. Notice that in the model (1), $J > ml^2$ and $\bar{M} > m$. Therefore, $\bar{M}J - m^2l^2 > 0$. For all non-zero system parameters the pair of matrices $(A, B)$ is controllable. Therefore, we can always choose a matrix $K$ such that $A + BK$ is Hurwitz. Consequently, we have found a controller solving the local output regulation problem. The controller (3) admits some freedom in the choice of the matrix $K$. This freedom can be used, for example, in tuning the controller to obtain desirable performance of the closed-loop system. Controller (3) is implemented in the experimental setup described in the next section.

## IV. Experimental setup

The experimental setup has been constructed by adapting an existing X-Y positioning system (the H-bridge setup) in the Dynamics and Control Technology Laboratory at Eindhoven University of Technology. The setup is shown in Fig. 2.

Fig. 2. The adapted H-bridge setup.

### A. Setup description

The adapted H-bridge setup is schematically shown in Fig. 3. It consists of the following components. The two parallel axes Y1 and Y2 are equipped with Linear Magnetic Motor Systems LiMMS Y1 and LiMMS Y2 that can move along their axes. These two carriages support the X-axis. In all experiments that are performed on this setup, the Y1 and Y2 carriages are controlled to maintain a fixed position with a low-level PID controller. Therefore, in the sequel we assume that these two carriages stand still and that the X-axis is fixed.

In the sequel we will refer to the X-LiMMS carriage moving along the X-axis as the cart. The mass of the cart is $M$ [kg]. The displacement of the cart $e$ [m] is measured using a linear incremental encoder (Heidenhain LIDA 201) with a 1 $\mu$m resolution. The force applied to the cart by the

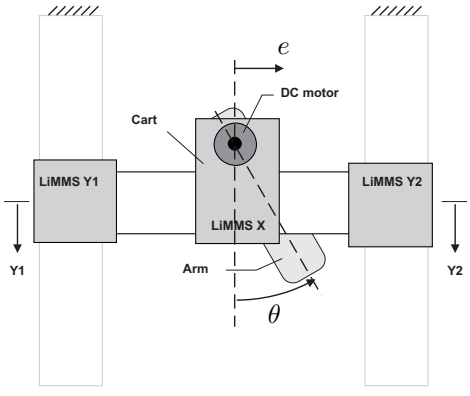


Fig. 3. The adapted H-bridge setup scheme, top view.

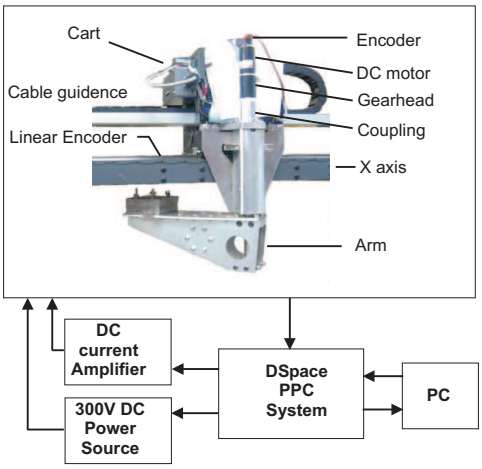


Fig. 4. The adapted H-bridge setup: rear view and connection scheme.

linear motor is proportional to the (voltage) control signal $u_F$ which is fed to the linear motor through a proportional current amplifier, i.e. $F = \kappa_F u_F$. The constant $\kappa_F$ has the value of 74.4 N/V ([16]). In addition to the actuating force, a friction force $F_f = F_f(\dot{e})$ is present in the roller bearings of the cart, which depends on the cart velocity. Moreover, there is a position dependent cogging force $F_c = F_c(e)$. This cogging force is caused by the interaction of the permanent magnets in the X-axis stator base and the iron-core coils of the electromagnets in the cart, see [16] for details.

In order to transform the $H$-bridge into a TORA system, additional hardware has been added to the cart, see Fig. 4. A vertical shaft supported by a set of (deep-groove and angular contact) ball bearings is attached to the back of the cart, thus forming a rotational joint. An arm of mass $m$ [kg] is attached to the lower end of the shaft. The center of mass of the arm is located at the distance $l$ [m] from the shaft center line. The angular position of the shaft (and consequently of the arm) $\theta$ is measured by a rotational incremental encoder (Maxon, HEDL55) with a (quadrature decoded) resolution of $0.18^\circ$ at the motor shaft. A 48V, 150W DC motor (Maxon RE40), fitted with a ceramic planetary gearhead (Maxon GP42C), drives the shaft via an adapted flexible coupling (ROBA-DX, type 931.333). The gear ratio $g_r$ equals 113. The backlash in the gearhead is approximately $0.5^\circ$ at the output shaft. The total inertia of all rotating parts (the arm, shaft, coupling, bearings, gearhead and motor) with respect to the shaft is $J$ [kg·m$^2$]. Due to the friction in the motor, gearhead and ball bearings of the shaft, an additional friction torque $T_f = T_f(\dot{\theta})$ acts on the arm. The torque $T_m$ generated by the DC motor is proportional to the current $i$ [A] fed to the motor, i.e. $T_m = \kappa_T i$, where $\kappa_T = 60.3$ mN $\cdot$ m/A is the motor constant. The current $i$ is generated by an analog current amplifier. It is proportional to the (voltage) control signal $u_T$ fed to the amplifier, i.e. $i = \kappa_A u_T$, where $\kappa_A = 1.6\,A/V$ is the amplifier constant.

Taking into account all the active forces and torques, we use the equations of Lagrange for the setup consisting of the cart moving along the fixed X-axis and the (horizontally)

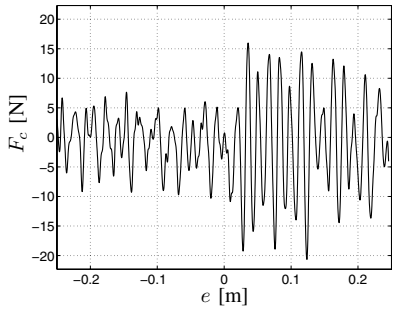


Fig. 5. The identified cogging force $F_c(e)$.

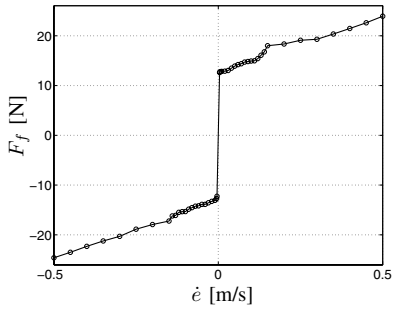


Fig. 6. The identified friction force $F_f(\dot{e})$.

rotating arm attached to the cart. The corresponding model has the following form

$$\begin{aligned} \bar{M}\ddot{e} + ml(\ddot{\theta}\cos\theta - \dot{\theta}^2\sin\theta) &= F - F_f(\dot{e}) + F_c(e), \\ J\ddot{\theta} + ml\ddot{e}\cos\theta &= T - T_f(\dot{\theta}), \end{aligned} \tag{7}$$

where $\bar{M} := M + m$, the actuator force acting on the cart equals $F = \kappa_F u_F$ and the actuator torque acting on the arm equals $T = g_r \kappa_T \kappa_A u_T$, where $u_F$ and $u_T$ are the control signals for the cart and for the arm, respectively.

The cogging force $F_c(e)$ and the friction force $F_f(\dot{e})$ have been identified using dedicated experiments [16], see Fig. 5 and 6, respectively. The friction torque $T_f(\dot{e})$ has been identified using constant angular velocity tests. The resulting graph is given in Fig. 7.

Initial estimates of the mass $\bar{M}$, the product $ml$ and the inertia $J$ are computed from the CAD drawings, material data and specifications of the motor and gearhead. These estimates are $\bar{M} = 20.965$ kg, $ml = 1.2514$ kg $\cdot$ m and $J = 0.5405$ kg·m$^2$. These estimates will be used as a starting

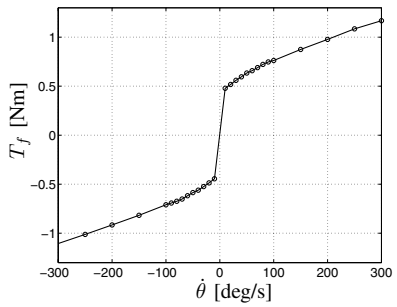


Fig. 7. The identified friction torque $T_f(\dot{\theta})$.

point to obtain more accurate estimates based on closed-loop experiments.

In order to implement the TORA system in the resulting setup, we need to compensate for the friction in the cart and the arm, and for the cogging force in the X-axis. Moreover, we need to implement the virtual spring action $-ke$ and the disturbance force $F_d$ along the X-axis. For the cart, this is achieved by the controller

$$u_F = \frac{1}{\kappa_F}(\hat{F}_f(\dot{e}) - \hat{F}_c(e) - ke + F_d), \tag{8}$$

where $\hat{F}_f(\dot{e})$ and $\hat{F}_c(e)$ are the friction compensation and cogging compensation forces (based on the identified values of these forces, see Fig. 6 and 5), $k$ [N/m] is the stiffness of the virtual spring (which we can set arbitrarily) and $F_d(t) = w_1(t)$ is the disturbance force acting on the cart. In the experiments performed on the setup, parameter $k$ is set equal to $k = 500$ N/m. The exosystem (2), with $w(t) = [w_1(t), w_2(t)]^T$, is integrated in the PC/dSpace-system and the disturbance force $F_d(t) = w_1(t)$ is computed from the obtained solutions.

Next, we need to implement friction compensation in the rotating arm. This is achieved by the controller

$$u_T = \frac{1}{g_r \kappa_T \kappa_A}(T_u + \hat{T}_f(\dot{\theta})), \tag{9}$$

where $\hat{T}_f(\dot{\theta})$ is the friction compensation torque based on the identified friction torque in the arm, see Fig. 7, and $T_u$ is a new control input.

After implementing the low-level controllers (8), (9) and the exosystem (2), the resulting system takes the form

$$\begin{aligned} \bar{M}\ddot{e} + ml(\ddot{\theta}\cos\theta - \dot{\theta}^2\sin\theta) + ke &= F_d + \varepsilon_F \\ J\ddot{\theta} + ml\ddot{e}\cos\theta &= T_u + \varepsilon_T, \end{aligned} \tag{10}$$

where $F_d(t) = w_1(t)$ is the disturbance force, $T_u$ is the control torque (new input) and $\varepsilon_F$ and $\varepsilon_T$ are the residual terms due to non-exact friction and cogging compensation and due to uncertainties in the system parameters. System (10) is now in the form of system (1) (if the residual terms are not taken into account) for which the controller (3) solves the local output regulation problem. This controller requires the values for $e$ and $\theta$, which are measured by the encoders, $\dot{e}$ and $\dot{\theta}$, which are obtained by numerical differentiation and filtering of the measured signals $e$ and $\theta$, and the values of $w_1(t)$ and $w_2(t)$, which are computed in the dSpace-system.

## V. Experiments

In this section we present experimental results performed on the adapted H-bridge setup in closed loop with the controller (9), (3).

### A. Parameter settings

The gain matrix $K$ in the controller (3) is set to $K := [29,\ -1.5,\ -11,\ -1.9]$. The eigenvalues of the linearized closed-loop system corresponding to this value of $K$ and to the estimated system parameters given in the previous section equal $-1.0313 \pm 5.8493i$ and $-0.9121 \pm 3.8901i$. The choice of the matrix $K$ is determined by several requirements. The first and the third entries in the matrix $K$, which correspond to the displacement of the cart $e$ and angular position of the arm $\theta$ must be large enough to compensate for the residual friction and backlash present in the system. At the same time, the real part of the eigenvalues of the linearized closed-loop system must be less than a certain threshold in order to guarantee fast convergence rates and sufficient robustness properties of the closed-loop system. Finally, the control signal resulting from this matrix $K$ must not exceed, in most operating conditions, the bounds imposed by the amplifier and $DC$ motor specifications. Taking these requirements into account, a combination of some optimization procedures with trial and error resulted in the matrix $K$ presented above.

The estimates for the parameters $J$ and $ml$ are tuned based on closed-loop experiments using the output regulation controller (in order to obtain better performance). The new estimates are $\hat{J} = 0.4270\ \mathrm{N\cdot m^2}$ (21% smaller than the initial estimate) and $\widehat{ml} = 1.3389\ \mathrm{kg\cdot m}$ (7% larger than the initial estimate). These estimates are used in the feedforward part of the output regulation controller in the experiments presented in this paper.

The friction compensation torque in the rotating arm $\hat{T}_f(\dot{\theta})$ is set 1.5 times larger than the identified friction torque $T_f(\dot{\theta})$ given in Fig. 7. It has been noticed that for this friction compensation in the rotating arm the controller has a better performance. Such a large deviation from the identified values may be explained by the fact that the friction in the gearhead, which is the main contributor to the friction in the arm motion, depends not only on the angular velocity $\dot{\theta}$, but also on the torque applied to the shaft. The identification of the friction torque has been performed for very low torques (constant velocity experiments), while in the experiments with the TORA controller the torques are much higher. The cogging compensation force $\hat{F}(e)$ is set equal to the identified cogging force presented in Fig. 5. The friction compensation force $\hat{F}_f(\dot{e})$ in the cart motion is set to 90% of the identified friction force presented in Fig. 6 to avoid overcompensation. Moreover, for a cart velocity $\dot{e}$ of magnitude less than $0.035$ m/s, it is set to

$$\hat{F}_f(\dot{e}) := \frac{|\dot{e}|0.90}{0.035} F_f(\dot{e}).$$

This under-compensation of the friction in the cart motion reduces the friction-induced limit-cycling which exceeds in experiments if the friction compensation force is set equal the real friction force, see e.g. [17]. At the same time, friction under-compensation makes the equilibrium set in terms of the position of the cart larger. In the experiments, this equilibrium set can be easily observed when the cart sticks in a point $e_*$, which is close, but not equal to zero.

In the experiments, the frequency of the disturbance force $F_d(t)$ (the frequency of the exosystem) is set to 1 Hz, which corresponds to $\omega$ in the exosystem (2) equal to $\omega = 2\pi$ rad/s.

| | $e_0$ [m] | $\theta_0$ [deg] |
|---|---|---|
| Experiment # 1 | -0.2 | 20 |
| Experiment # 2 | 0.2 | 20 |
| Experiment # 3 | 0.1 | 90 |

TABLE I

INITIAL CONDITIONS $e_0$ AND $\theta_0$ USED IN THE EXPERIMENTS.

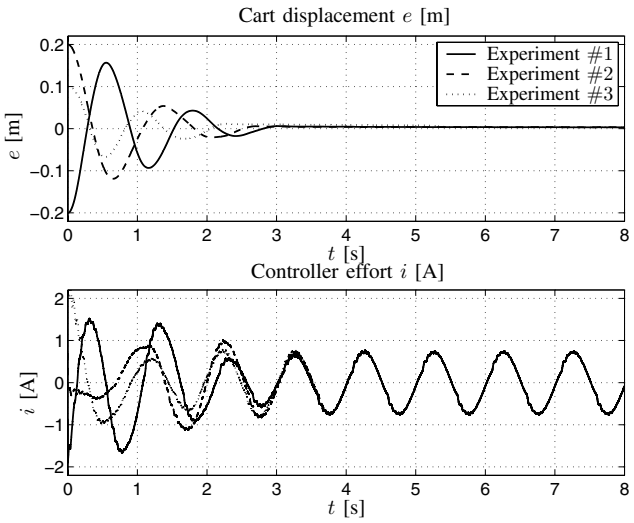


Fig. 8. Experiments for a disturbance force of amplitude $\mathcal{A} = 15$ N and predefined initial conditions.

### B. Experimental results

All experiments are performed for the initial conditions of the exosystem equal to $w_1(0) = 0$, $w_2(0) = \mathcal{A}$. These initial conditions correspond to the disturbance force $F_d(t) := \mathcal{A}\sin(\omega t)$. We perform the experiments for two values of the amplitude $\mathcal{A}$: $\mathcal{A} = 15$ and $\mathcal{A} = 25$ N.

Two types of experiments are performed. In the experiments of the first type, the system starts in a given initial condition $e(0) = e_0$ [m], $\dot{e}(0) = 0$ [m/s], $\theta(0) = \theta_0$ [deg], $\dot{\theta}(0) = 0$ [deg/s]. For each value of the amplitude $\mathcal{A}$ we perform three experiments corresponding to different initial conditions $e_0$ and $\theta_0$. These initial conditions are given in Table I. The results of the experiments corresponding to the disturbance amplitudes $\mathcal{A} = 15$ and $\mathcal{A} = 25$ N are presented in Fig. 8 and 9, respectively. In these figures the controller effort is represented by the current $i = \kappa_A u_T$ [A] fed by the amplifier to the DC motor.

In the experiments of the second type, the system is affected once again by a disturbance force $F_d(t)$ of amplitude $\mathcal{A}$. Initially, only the feedback part in the controller (3) is active, i.e. $T_u = Kx$, and there is no compensation for the disturbance force $F_d(t)$. Since there is no disturbance compensation, the cart starts oscillating. At an arbitrary time instant $t_*$ the feedforward part of the controller is activated, i.e. $T_u = c(w) + K(x - \pi(w))$. This results in disturbance rejection in the position of the cart $e$. The results of the experiments corresponding to the disturbance amplitudes $\mathcal{A} = 15$ and 25 N are presented in Fig. 10 and 11, respectively.

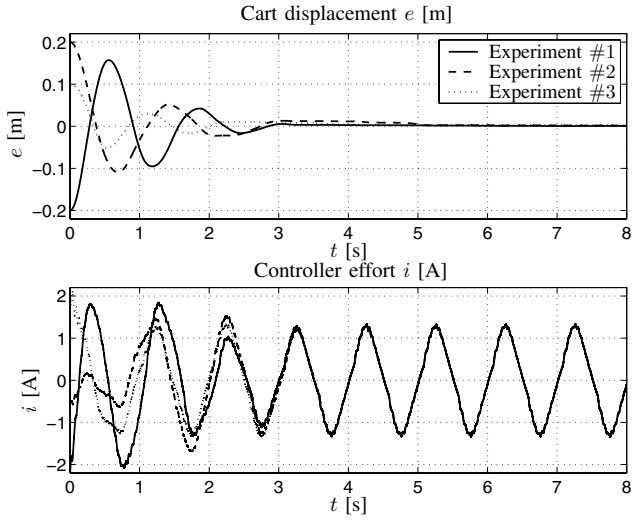


Fig. 9. Experiments for a disturbance force of amplitude $\mathcal{A} = 25$ N and predefined initial conditions.

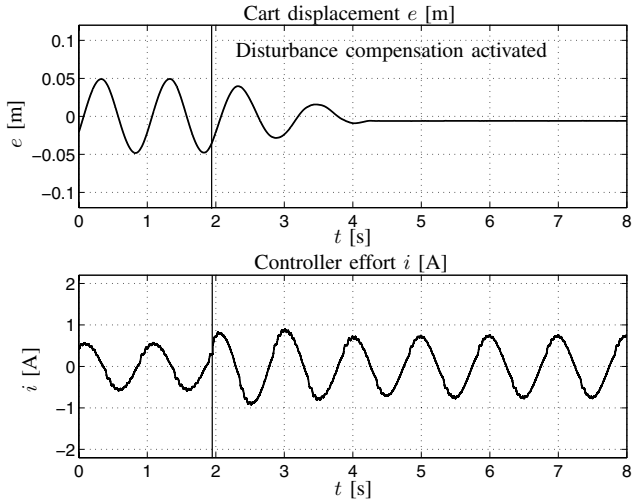


Fig. 10. Experiments for a disturbance force of amplitude $\mathcal{A} = 15$ N. Disturbance compensation is activated during the experiment.

From these experimental results we can immediately draw the following conclusion. The output regulation controller (3) does compensate a significant part of the harmonic disturbance force acting on the cart, and the output regulation occurs. The residual friction in the cart motion manifests itself in the sticking phenomenon: after transients the cart stabilizes at an equilibrium position which is close, but not equal to zero.

In Fig. 12 the cart displacement signal related to an experiment, performed at a different time, is depicted. Clearly, exact output regulation is not attained and a limit cycle of small amplitude remains. In this respect, it should be noted that the friction characteristics in the setup are subject to change due to temperature and humidity change in the laboratory. However, exactly the same friction compensation as in the previous experiments was used. Consequently, the limit cycling can be caused by an interaction of several

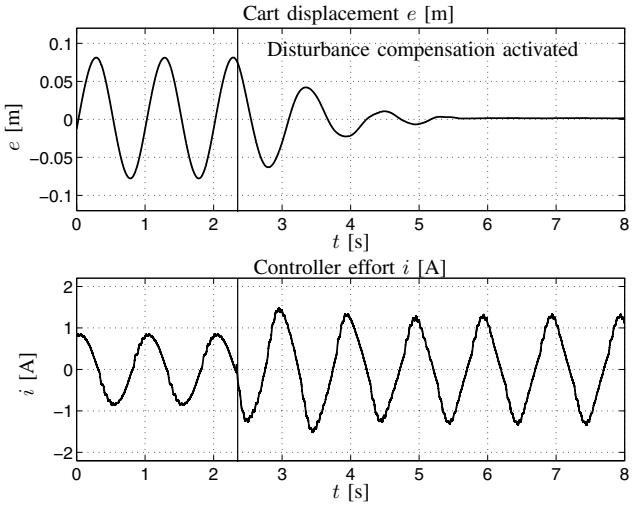


Fig. 11. Experiments for a disturbance force of amplitude $\mathcal{A} = 25$ N. Disturbance compensation is activated during the experiment.

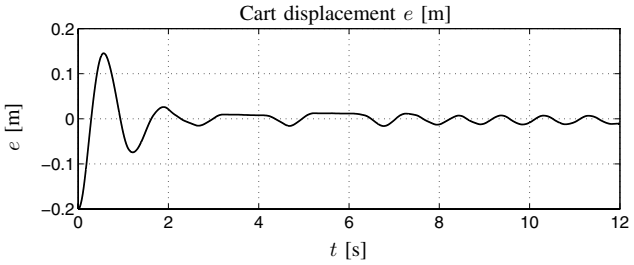


Fig. 12. Limit cycling in the cart motion. The disturbance force amplitude is $\mathcal{A} = 15$ N.

factors: friction and friction compensation in the cart motion, friction and friction compensation in the rotating arm, feedback controller and backlash in the gearhead. These problems require an additional investigation which is outside the scope of our research.

## VI. Conclusions

In this paper we have presented experimental results on the local output regulation problem for the TORA system. First, we have constructed a simple state-feedback controller which solves a disturbance rejection problem for the TORA system. This problem is a particular case of the local output regulation problem. In order to validate this controller in experiments, an experimental setup for the TORA system has been built from an existing H-bridge setup. The proposed state-feedback controller has been implemented in this setup and tested in a row of experiments.

As follows from the results of these experiments, for the setup in closed loop with the proposed controller, output regulation occurs, though only approximately. This means that the regulated output $e(t)$ does not tend to zero exactly, but either sticks in an equilibrium position close to zero or keeps on oscillating with a small amplitude. These phenomena are due to non-exact compensation of the friction and due to the backlash problem in the gearhead of the rotating arm.

In practice there is always some type of (non-)parametric uncertainty present in the system. It can be either due to inaccurately identified parameters of the system or due to friction, backlash or other parasitic phenomena acting on the system, which are not taken into account in the system model. These uncertainties may significantly reduce the performance of a controller. This performance deterioration may manifest itself, for example, in a steady-state regulation error, as illustrated by the experimental results on the TORA system presented above. It should be noted that most theoretical works on robust output regulation for nonlinear systems are focused mainly on parametric uncertainties. The results presented in this paper urge the need for further work on the robustness of output regulation controllers with respect to non-parametric uncertainties.

The results given in this paper represent one of the first steps in the field of experimental output regulation for nonlinear systems. They illustrate applicability of the nonlinear output regulation theory in experiments. Further work is under way to implement an output-feedback controller for the disturbance rejection problem and to reduce the sticking and limit cycling phenomena caused by friction and backlash.

## References


[1] B. Francis and W. Wonham, "The internal model principle of control theory," *Automatica*, vol. 12, pp. 457–465, 1976.

[2] E. Davison, "Multivariable tuning regulators: the feedforward and robust control of a general servomechanism problem," *IEEE Trans. Automatic Control*, vol. 21(1), pp. 35–47, 1976.

[3] A. Isidori and C. Byrnes, "Output regulation of nonlinear systems," *IEEE Trans. Automatic Control*, vol. 35, pp. 131–140, 1990.

[4] J. Huang and W. Rugh, "An approximation method for the nonlinear servomechanism problem," *IEEE Trans. Automatic Control*, vol. 37(9), pp. 1395–1398, 1992.

[5] A. Isidori, L. Marconi, and A. Serrani, *Robust autonomous guidance*. London: Springer, 2003.

[6] J. Huang, *Nonlinear output regulation. Theory and applications*. Philadelphia: SIAM, 2004.

[7] Z. Lin, M. Glauser, T. Hu, and P. E. Allaire, "Magnetically suspended balance beam with disturbances: a test rig for nonlinear output regulation," in *Proc. of IEEE Conf. Decision and Control*, 2004.

[8] C. Bonivento, A. Isidori, L. Marconi, and A. Paoli, "Implicit fault-tolerant control: application to induction motors," *Automatica*, vol. 40(3), pp. 355–371, 2004.

[9] C.-J. Wan, D. Bernstein, and V. Coppola, "Global stabilization of the oscillating eccentric rotor," in *Proc. of IEEE Conf. Decision and Control*, 1994.

[10] Z.-P. Jiang and I. Kanellakopoulos, "Global output-feedback tracking for a benchmark nonlinear system," *IEEE Trans. Automatic Control*, vol. 45, pp. 1023–1027, 2000.

[11] A. Pavlov, N. van de Wouw, and H. Nijmeijer, "The local output regulation problem: convergence region estimates," *IEEE Trans. Automatic Control*, vol. 49(5), pp. 814–819, 2004.

[12] J. Huang and G. Hu, "A control design for the nonlinear benchmark problem via the output regulation method," *J. Control Theory and Applications*, vol. 2(1), pp. 11–19, 2004.

[13] A. Pavlov, "The output regulation problem: a convergent dynamics approach," Ph.D. dissertation, Eindhoven University of Technology, Eindhoven, 2004.

[14] C. Byrnes, F. D. Priscoli, and A. Isidori, *Output regulation of uncertain nonlinear systems*. Boston: Birkhauser, 1997.

[15] A. Isidori, *Nonlinear control systems, 3rd ed.* London: Springer-Verlag, 1995.

[16] R. Hensen, "Controlled mechanical systems with friction," Ph.D. dissertation, Eindhoven University of Technology, Eindhoven, 2002.

[17] D. Putra, "Control of limit cycling in frictional mechanical systems," Ph.D. dissertation, Eindhoven University of Technology, Eindhoven, 2004.